Korean J. Chem. Eng., 37(1), 130-140 (2020)
DOI: 10.1007/s11814-019-0405-9

pISSN: 0256-1115
eISSN: 1975-7220

Low temperature adsorption of nitric oxide on cerium impregnated biomass-derived biochar

Shahreen Izwan Anthonysamy*, Pooya Lahijani*, Maedeh Mohammadi, and Abdul Rahman Mohamed*,†**

*Low Carbon Economy (LCE) Research Group, School of Chemical Engineering, Universiti Sains Malaysia, 14300, Nibong Tebal, Pulau Pinang, Malaysia
**Faculty of Chemical Engineering, Babol Noshirvani University of Technology, Babol 47148, Iran
(*Received 17 June 2019 • accepted 12 October 2019*)

Abstract−This study investigates the catalytic oxidation of NO to NO_2 over biomass-derived biochar at ambient temperature. Rubber seed shell (RSS) was used as lignocellulosic waste to develop biochar for NO capture. The NO adsorption capacity of pristine biochar was low, about 17.61 mg/g at 30 °C. To enhance the NO uptake capacity of biochar, cerium (Ce) was introduced into the biochar surface through simple impregnation method. Upon this, the NO adsorption capacity of 3 wt% Ce-loaded biochar profoundly increased to 75.59 mg/g at the same adsorption condition. This was confidently due to the excellent oxygen storage capacity of ceria which could react with free active sites on the biochar surface to form oxidized cites C(O). Characterization results indicated that the adsorbed species was in the form of -O-N=O, suggesting that the adsorption of NO was followed by reaction with surface oxidized sites to form NO_2. Studying the kinetics of the NO adsorption using pseudo-second order, Avrami and Elovich models showed that chemisorption was the chief mechanism that governed the adsorption process and the activation energy for NO adsorption was estimated to be around −45 kJ/mol.

Keywords: Biochar, Rubber Seed Shell, NO Adsorption, Ceria, Chemisorption

INTRODUCTION

Nitrogen oxides (NO_x), including nitric oxide (NO) and nitrogen dioxide (NO_2), are highly toxic gases and are considered important air pollutants. They are emitted from anthropogenic sources such as power plants, transportation and industries. In fact, NO is produced during the combustion of fossil fuels, it is then oxidized in the atmosphere to NO_2 which is a more toxic and irritating gas [1]. These toxic gases produce acid rains and photochemical smog and hence contribute to the current climate change crisis [2,3]. Thus, reduction of emission of NO_x into the atmosphere is a major environmental concern.

One of the most studied and mature techniques for the removal of NO_x from flue gas is selective catalytic reduction (SCR) [4,5]. This method converts the toxic NO_x to inert N_2 through reduction process in the presence of reducers such as ammonia and urea [5,6]. The conversion, however, is carried out under relativity harsh processing condition where use of excess oxygen is also required [7]. The SCR catalysts (palladium and platinum oxides), besides being expensive, are efficient at high reaction temperatures (>300 °C) [5,8], which is far beyond the temperature of exhaust gas (~100 °C) from a fossil power plant [7]. Moreover, there is a high possibility of NH_3 leakage and formation of hydrogen cyanide (HCN), which adds to the drawbacks of the process. Although catalytic reduction of NO_x is still deployed at commercial scale, due to the very low concentration of NO_x gases (<0.1%), catalyst poisoning or inhibition by other coexisting gases in the flue gas has remained a challenge [9]. Alternatively, the adsorption process can be used as a simple and easily controlled method for NO_x sequestration and decomposition.

NO is the major component of NO_x, comprising 85-90% of the total [8,10]. Since NO is a supercritical fluid at the ambient condition, its physical adsorption on porous adsorbents is restricted, attributing to its weak interaction with the adsorbent. In this context, catalytic oxidation of NO to NO_2 on the carbon surface at ambient condition and then condensation of NO_2 in the pores of adsorbent sounds promising. This process is chemically benign and allows for the removal of NO from flue gas at ambient temperature, although it presents at near-trace levels (300-1,500 ppm) [7] compared to the other constituents of combustion flue gas. The extent of physical adsorption of NO on carbon materials is tremendously lower than the amount that NO_2 could be adsorbed. This is because the van der Waals constant, *a*, for NO_2 is almost four-times higher than that for NO [9]. Hence, NO should be oxidized to NO_2 at the carbon surface and then condense in the pores. The surface oxidation of NO becomes possible in the presence of oxygen, either adsorbed on the surface or molecular in the gas phase [11]. The condensed NO_2 in the pores can then be desorbed and beneficially used as a precursor for the synthesis of chemicals such as nitric acid [12], or as an intermediate for production of products such as agricultural nitrates [7].

It has been reported that carbon materials can serve as a catalyst to convert NO to NO_2 in the presence of oxygen [5,11]. In fact, the carbon defects and dangling bonds at the edge of char structure can act as catalytic active sites for the conversion of NO to NO_2

†To whom correspondence should be addressed.
E-mail: chrahman@usm.my

while oxygen also is present [5]. Introduction of ceria (CeO_x) into the surface of adsorbent has been found as an efficient route for enhancing the oxidation of NO to NO_2 or NO decomposition, owing to the excellent oxygen storage capacity of CeO_x [6,13,14]. Ceria has the ability of transition between Ce^{4+} and Ce^{3+} and oxygen vacancy creating and filling under redox condition [15]. This redox cycle can provide excess adsorbed oxygen on the carbon surface and strengthen the conversion of NO to NO_2, which ultimately results in improved uptake capacity of the adsorbent [16].

So far, various carbon-based materials including activated carbon [5,11,17-20] and phenolic resin-based mesoporous carbon [6,13] have been used for catalytic oxidation of NO to NO_2 at low temperature. Development of adsorbent from low cost and sustainable resources that exhibit high NO_x uptake capacity at relatively low temperature would enhance the economical and practical feasibility of the NO_x removal process. In this context, this study investigated the adsorption of NO using biomass-derived biochar at ambient condition. To the best of authors' knowledge, studies on the removal of NO_x using biochar sorbents at ambient temperature are very scarce. Rubber seed shell (RSS), which is the leftover residue after separation of oil from rubber seed kernel, was used as a plentifully available and low cost lignocellulosic waste to develop biochar through fast pyrolysis. Ce-containing biochars were then prepared by wetness impregnation method. The pristine and Ce-loaded biochars were used for NO capture at ambient condition through isothermal thermogravimetric method. The adsorption kinetics was also studied to find the governing adsorption mechanism.

Table 1. Proximate and ultimate analyses of RSS biomass and its ash composition

Parameter	Value
Proximate analysis (wt%, dry basis)	
Volatiles	77.70
Ash	0.40
Fixed carbon	21.90
Ultimate analysis (wt%)	
Carbon	48.36
Hydrogen	5.75
Nitrogen	0.14
Sulfur	0.30
Oxygen*	45.45
Ash analysis (wt%, dry basis)	
SiO_2	6.63
TiO_2	0.39
Al_2O_3	3.41
Fe_2O_3	1.48
MnO	0.17
MgO	2.37
CaO	8.42
Na_2O	0.51
K_2O	67.79
P_2O_5	4.94
SO_3	2.53
Trace elements (μg/g)	Cl, Cr, Cu, Mo, Nb

*Calculated by difference

MATERIALS AND METHODS

1. Biomass and its Characteristics

Rubber (*Hevea brasiliensis*) seed shell used for the development of biochar was obtained from a rubber plantation area in Serdang, Perak, Malaysia. The shells were cleaned, washed and dried in an oven at 105 °C overnight. The dried shells were crushed using a mechanical crusher and stored as the feedstock for biochar preparation. To measure the moisture, volatile, ash and fixed carbon content of the RSS, proximate analysis was carried out using a thermogravimetric analyzer (TGA, SDTQ-600). The elemental composition of the RSS was determined using an elemental analyzer (PerkinElmer 2400 Series II CHNS/O). The ash composition of RSS was analyzed using X-ray Fluorescence analyzer (XRF, PanAlytical Axios Max). The characterization results are summarized in Table 1.

2. Preparation of Pristine and Ce-loaded RSS Biochars

RSS biochar was produced in a carbonization unit by pyrolyzing the biomass under a continuous supply of nitrogen. RSS samples were pyrolyzed at different carbonization temperatures of 500, 700 and 900 °C for 90 min and the obtained biochars were denoted as RSS500, RSS700 and RSS900, respectively. The biochar yield from the RSS pyrolyzed at 500, 700 and 900 °C was found to be 19.68, 13.74 and 7.13%, respectively. All the developed RSS biochar samples were then pulverized and sieved to a particle size of 63 μm and stored in air-tight containers for subsequent experiments. Selection of such particle size was based on a set of preliminary experiments carried out using biochars with different particle sizes to find the particle size using which the highest NO uptake capacity could be attained (Fig. S1).

For preparation of metal-doped biochar, the RSS biochar was impregnated with cerium nitrate solution and then calcined under N_2 to obtain cerium oxide-loaded biochar. To this end, calculated quantities of cerium (III) nitrate hexahydrate ($Ce(NO_3)_3{\cdot}6H_2O$) were dissolved in 100 ml of deionized water to have various concentrations of metal solution (1, 3, 5 and 8 wt%). One g of the RSS biochar was then added into the metal solution and stirred for 24 h. Then, the cerium impregnated RSS biochar was dried overnight. Ultimately, the dried metal impregnated biochar was calcined under N_2 at 500 °C to obtain cerium oxide (CeO_2)-doped biochar. Preliminary experiments on the effect of calcination temperature (400, 500, 600 and 700 °C) indicated that the temperature of 500 °C was suitable to develop a sorbent with high NO uptake capacity (Fig. S2), so this calcination temperature was used in preparation of all Ce-loaded biochar samples.

3. Nitric Oxide Adsorption Test

NO adsorption tests were conducted in a thermogravimetric analyzer (TGA, SDTQ-600). In each experiment, around 6 to 8 mg of RSS biochar, either as-produced or cerium-impregnated, was loaded in a ceramic pan and heated under nitrogen gas (75 ml/min) to 120 °C and kept at this temperature for 20 min to remove any moisture or gases which might be adsorbed by the biochar. Then, the RSS biochar was cooled under nitrogen gas to the desired adsorption temperature (30, 40, 50 and 70 °C). At the onset of the adsorp-

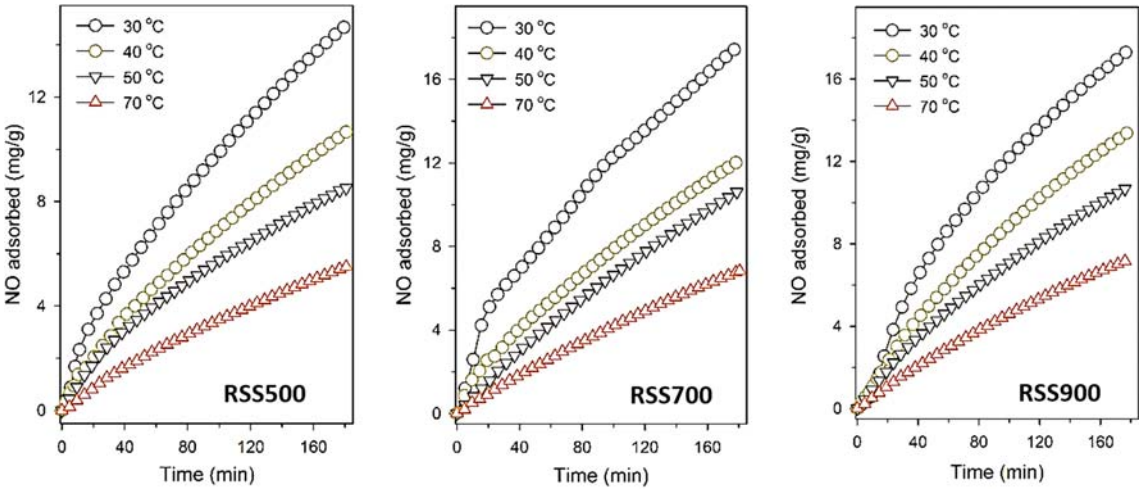

Fig. 1. Effect of pyrolysis temperature on the NO adsorption capacity of RSS biochar at different adsorption temperatures.

tion test, nitrogen gas was switched to a mixed gas (75 ml/min) containing 2,000 ppm of NO in N_2; the biochar adsorbent was exposed to this gas under the isothermal condition for 180 min. The variations in the weight of biochar were continuously recorded as a function of time to calculate the NO adsorption capacity in mg/g. To ensure that the observed variations in sample weight were attributed to the NO adsorption, not N_2 capture, similar adsorption tests were repeated using pure N_2 gas, as control test. To analyze the regeneration performance of the biochar, some cycles of NO uptake and release were tested. For this purpose, the selected biochar sample was exposed to the gas containing 2,000 ppm NO for 180 min, then the gas was switched to N_2 and the temperature was raised to 220 °C for 35 min for desorption. The tests for adsorption and desorption of NO were repeated twelve times and the changes in the sample weight were recorded instantaneously. To ensure the repeatability of the results, the experiments were replicated twice.

4. Analytical Methods

The surface functional groups of the RSS biochars were analyzed using a Thermo Scientific Nicolet iS10 Fourier transform infrared (FTIR) spectrometer. To analyze the morphology of the developed biochars and to determine the surface chemical composition the biochar samples, a Quanta 450 FEG Scanning electron microscope (SEM) equipped with an energy dispersive spectrometer (EDS) was used. To gain an insight into the intrinsic carbon structure of the prepared biochars, the samples were analyzed using a Renishaw inVia Raman spectrometer. To analyze the state and concentration of the elements on the biochar surface, X-ray photoelectron spectroscopy (XPS) was carried out on the biochar samples, before and after adsorption. The data were obtained using a ULVAC-PHI Quantera II XPS equipped with an Al Kα X-ray source (hv=1,486.6 eV).

RESULTS AND DISCUSSION

1. NO Uptake by Pristine RSS Biochar

To study the effect of pyrolysis temperature on the NO adsorption capacity, the RSS biochars prepared at different carbonization temperatures (500, 700 and 900 °C) were subjected to the NO adsorption; the adsorption tests were conducted at different temperatures from 30 to 70 °C, and the results are presented in Fig. 1. All biochar samples revealed almost similar adsorption trend where the NO uptake was continuously increasing and did not approach an asymptotic value within 180 min. The absence of plateau on the adsorption isotherms implies that the maximum uptake capacity was not reached in any condition and the biochars were not saturated by the NO_x gases. The NO capture capacity of biochars also followed a decreasing trend with increase of adsorption temperature from 30 to 70 °C for all biochar samples. This impact of temperature on the gas uptake was associated with the decrease of the van der Waals attraction with increase of temperature that adversely affected the adsorption capacity. The highest NO uptake at 0.2% concentration in mixed gas was 14.80, 17.61 and 17.78 mg/g for RSS500, RSS700 and RSS900, respectively, at 30 °C. The amount of N_2 adsorbed at 30 °C (referred to as control) by all biochar samples was low, around 3 mg/g. Since the kinetic diameters of N_2 (0.364 nm), NO (0.317) and NO_2 (0.340 nm) differ only slightly any pore filling by these gases because of steric effects is expected to be negligible. However, micropore filling has been reported to be only effective for gases whose crtitical temperatures (T_C) are above the implemented adsorption temperature [9]. Considering that the T_c of N_2, NO and NO_2 is 126, 180 and 431 K, respectively, only the T_C of NO_2 is higher that the used adsorption temperatures in this study (303 to 343 K). Accordingly, at atmospheric pressure the adsorption of N_2 and NO in micropores is insignificant compared to the adsorbed NO_2. Moreover, the extent of micropore filling in carbon material is known to be in correlation with the van der Waals constant *a* [9]. This constant for NO_2 is approximately four-times gretaer than that for N_2 and NO; this makes NO_2 as the preferred adsorbated over N_2 and NO.

According to the results presented in Fig. 1, increase of the pyrolysis temperature from 500 to 700 °C was effective to enhance the NO uptake capacity, yet upon further increase of the carbonization temperature to 900 °C the NO adsorption capacity increased only

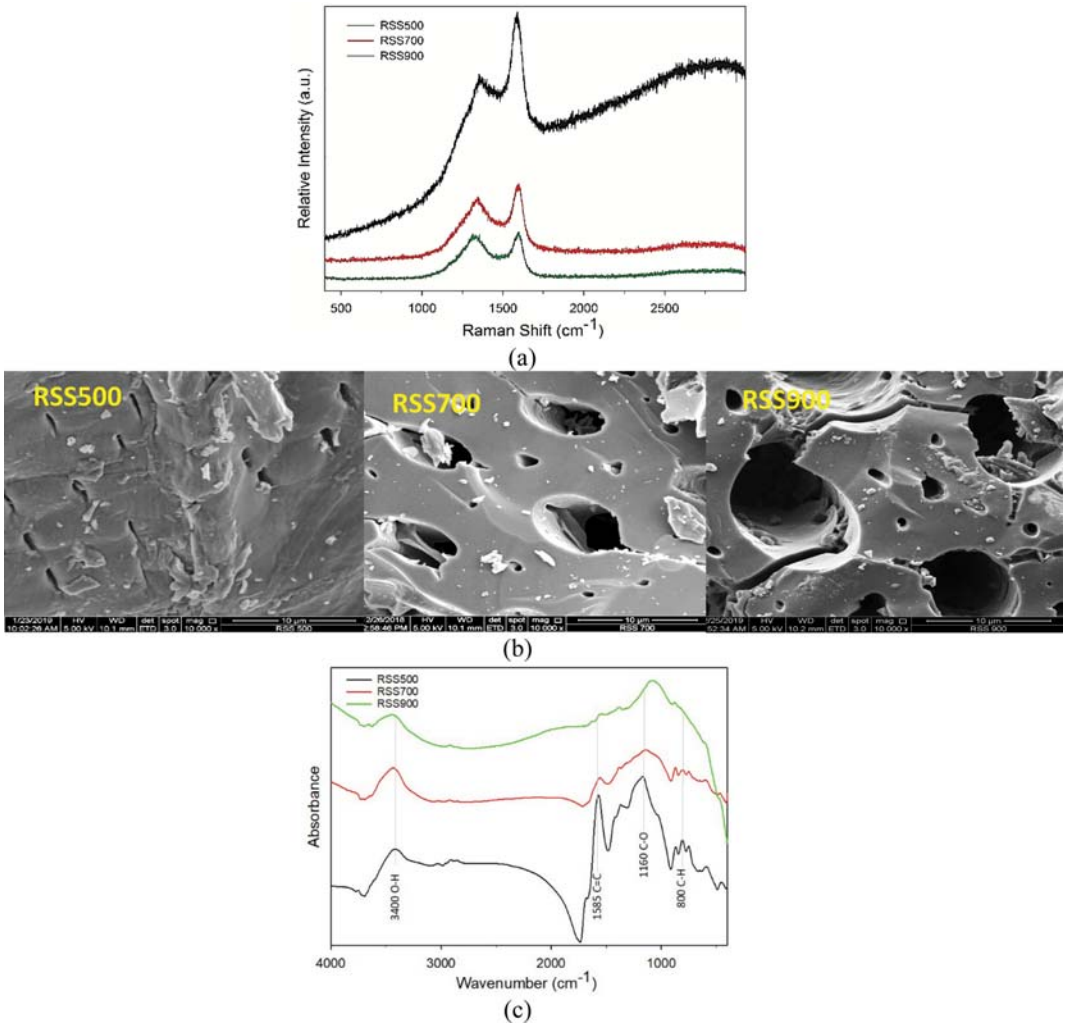

Fig. 2. (a) Raman spectra, (b) SEM micrographs and (c) FTIR spectra of RSS biochars prepared at different pyrolysis temperatures.

marginally at all adsorption temperatures. The variations in the NO uptake capacity of biochars developed at different carbonization temperatures should be associated with the structural evolutions and transformations that take place during pyrolysis. In this sense, several characterization analyses were carried out on the biochar samples to study the structural alterations and reformations of char particle in the course of pyrolysis.

The influence of pyrolysis temperature on the carbon structure of the RSS biochars was analyzed by Raman spectroscopy. Fig. 2(a) shows the Raman spectra of the RSS biochar samples developed at different pyrolysis temperatures. As observed, the Raman spectra of the three biochars are dissimilar, indicating the significant influence of carbonization temperature on the structural features of the biochars. In all spectra, two characteristic peaks are observed around 1,350 and 1,590 cm^{-1}, which respectively indicate the amorphous (*D*-band) and crystalline (*G*-band) phases of the biochar structure. With increase of the carbonization temperature from 500 to 900 °C, the intensity of both peaks reduced. Nevertheless, the intensity of *D*-band (I_D) increased over *G*-band (I_G) signifying that with increase of pyrolysis temperature the share of amorphous carbon increased. At the carbonization temperatures of 500, 700 and 900 °C, the I_D/I_G was 0.78, 0.86 and 0.97, respectively. This growing ratio is indicative of the development of amorphous phase in the biochar along with increase of pyrolysis temperature, where the symmetry of carbon structure was broken down and the share of disordered carbon increased. Due to such structural changes and development of defective structure in the course of high temperature pyrolysis, it is reasonable to expect some alteration in pore and microstructure of the biochars. To confirm this premise, the surface morphology of the RSS biochars prepared at different carbonization temperatures was analyzed by SEM. Fig. 2(b) exhibits the SEM micrographs of the RSS biochars wherein porosity development and enlarging of the pores along with increase of the carbonization temperature are noticeably observed. It was interesting that despite porosity development and creation of more defects (as confirmed by Raman analysis) with increment of pyrolysis temperature, the NO uptake capacity of RSS900 was almost identical to that of RSS700 at all adsorption temperatures. To justify this behavior, it is worth to discuss that high temperature pyrolysis can cause the formation of new micropores due to fragmentation of biochar particles while undergoing devolatilization. Yet, high temperature can result in excess widening and enlarging of the existing pores, as evidenced

by SEM micrographs. According to the literature [7], there is a relationship between the pore size/structure and the uptake of NO_2 and the condensation of NO_2 is presumably favored in micropores of carbons. Therefore, it could be speculated that the excess heating of the biochar although contributing to the porosity development and creation of new pores, however, adversely affected the existing microporous structure, which significantly contributed to the sorption and condensation of gas molecules, by enlarging the pores. It is also plausible that the surface chemical groups of biochar, which contribute to the gas uptake, were affected by high temperature. Thus, to study the influence of pyrolysis condition on the development or loss of surface functional groups, the RSS biochars, which were prepared at different pyrolysis temperatures, were subjected to FTIR analysis. Fig. 2(c) depicts the FTIR spectra of the developed biochars. The peak located around 3,400 cm^{-1} is associated with the O-H stretching vibrations of carboxyl or hydroxyl groups. The intense peak near 1,585 cm^{-1} can be attributed to the C=C vibrations in aromatic ring structures [19]. The wide peak observed around 1,160 cm^{-1} is most probably assigned to the C-O stretching vibrations in ether or ester groups [21]. The band around 800 cm^{-1} can be associated with the vibration of C-H in the aromatic ring. With increase of the carbonization temperature, the intensity of these characteristic peaks reduced and some of the bands disappeared. This observation signifies that high temperature pyrolysis destroyed some of the surface chemical functional groups which could play role in the NO uptake process. According to the characterization results, it can be concluded that use of high temperature (900 °C) was effective to develop the porosity of biochar and creation of defects and new pores, yet the existing pores were widened and some of the surface chemical groups were destroyed at high temperature. Because of these effects, the NO uptake capacity of RSS900 did not improve compared to that of RSS700. Accordingly, it can be concluded that both the pore structure and surface chemical groups may be important for selective sorption of NO. In the following, RSS700 with similar uptake capacity to that of RSS900 was used as the platform for development of efficient sorbent with high NO uptake capacity.

2. NO Uptake by Cerium-loaded RSS Biochar

In an effort to enhance the NO capture capacity of RSS biochar, selected biochar sample (RSS700) with the NO uptake capacity of 17.61 mg/g at 30 °C was impregnated with several concentrations of cerium solution. The introduction of cerium into the biochar surface, as confirmed by SEM-EDS analysis (Fig. 3), provides excess adsorbed oxygen atoms. These surface oxygen atoms react with active sites on the biochar surface to form more surface oxygen functional groups which are very beneficial for NO adsorption

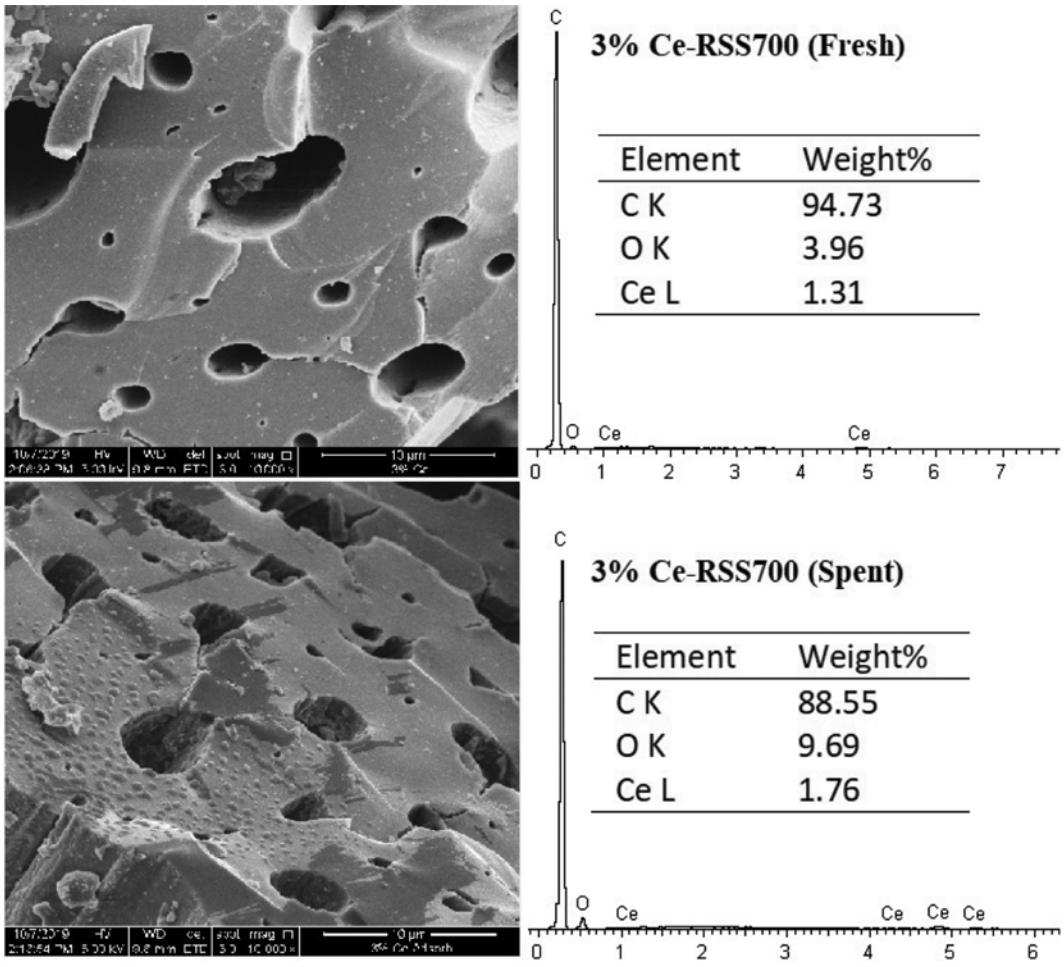

Fig. 3. SEM-EDS analysis of 3% Ce-RSS700 before (fresh) and after (spent) NO adsorption.

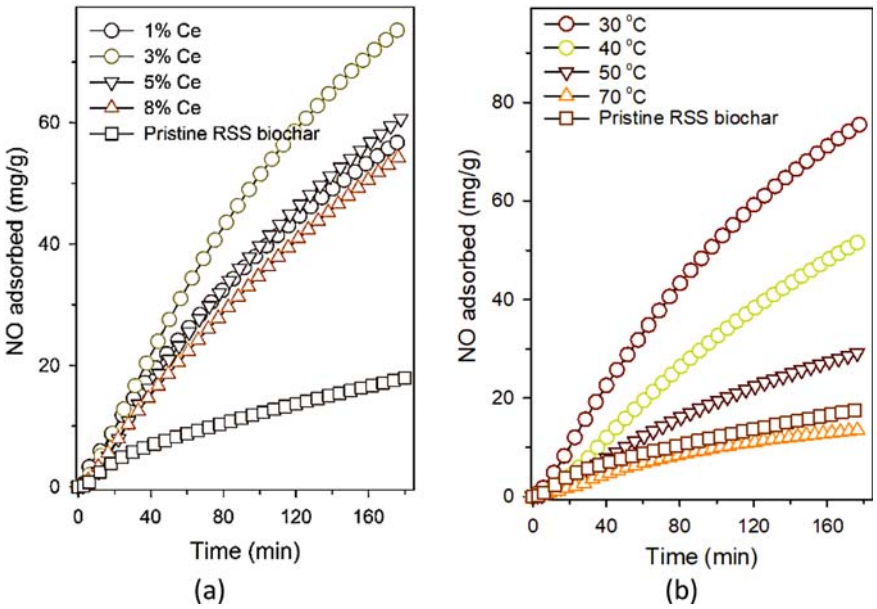

Fig. 4. NO uptake capacity of (a) Ce-loaded RSS700 with different Ce contents at 30 °C and (b) 3% Ce-loaded RSS700 at different adsorption temperatures.

and/or NO oxidation to NO_2; as a result, the NO uptake capacity of the cerium-loaded biochar increases. The NO uptake capacity of Ce-loaded biochar is exhibited in Fig. 4(a). The NO capture capacity of biochar was considerably enhanced upon the introduction of Ce into the biochar surface; all Ce-loaded biochars revealed higher capture capacity compared to that of pristine biochar, with 3% Ce-loaded biochar leading other samples. The adsorption capacity of 3% Ce-RSS700 (75.59 mg/g) was more than four-times that of pristine biochar (17.61 mg/g); this indicates the great impact of cerium on enhancement of NO uptake, possibly through oxidation of NO to NO_2, which is discussed in the following. With increase of cerium loading from 1 to 3 wt%, the uptake capacity improved considerably, yet with further increase of cerium loading to 5 and then 8 wt%, the adsorption capacity dropped. This was possibly caused by the agglomeration of CeO_2 particles at higher loadings, which could lead to the poor dispersion of CeO_2 on the biochar surface and adversely affect the NO adsorption. Fig. 4(b) shows the NO uptake capacity of 3% Ce-RSS700 at different temperatures. As expected, with increase of the adsorption temperature from 30 to 70 °C, the NO uptake capacity dropped from 75.59 to 13.60 mg/g, indicating the exothermic nature of the adsorption process. The SEM-EDS analysis 3% Ce-RSS700 after NO adsorption (Fig. 3) did not show any notable morphological changes in the structure of biochar. The increase in the surface oxygen composition after adsorption could be attributed to the chemically bound NO_2 to the biochar surface.

In a previous study [22] which was conducted for the simultaneous removal of SO_2 and NO from a simulated flue gas using cerium impregnated (10 wt%) palm shell-based activated carbon at 150 °C, the sorption capacity of 121.7 and 3.5 mg/g was achieved for SO_2 and NO, respectively. Cao et al. [13] reported an NO adsorption capacity of 16.35 mg/g on ordered mesoporous carbon (OMC) at 50 °C; upon introduction of cerium into the OMC structure (2 wt%) the adsorption capacity increased to 18.61 mg/g. In another study by the same group of researchers [13], NO adsorption capacity of 19.40 and 22.00 mg/g was reported for the OMC and 2 wt% Ce-loaded OMC, respectively. Guo et al. [5] reported an NO adsorption capacity of 23 mg/g for coconut shell-based activated carbon at 120 °C. Comparison of the results of the current study to those available in the literature signifies the considerably higher NO adsorption capacity (75.59 mg/g) obtained using 3% Ce-loaded biochar at ambient temperature (30 °C).

To identify the possible mechanism for adsorption of NO on the biochar, the changes in the surface chemical properties of pristine (RSS700) and Ce-doped biochar (3% Ce-RSS700), before and after NO adsorption, were studied by FTIR analysis as shown in Fig. 5. Comparison of the FTIR spectra of pristine and Ce-loaded

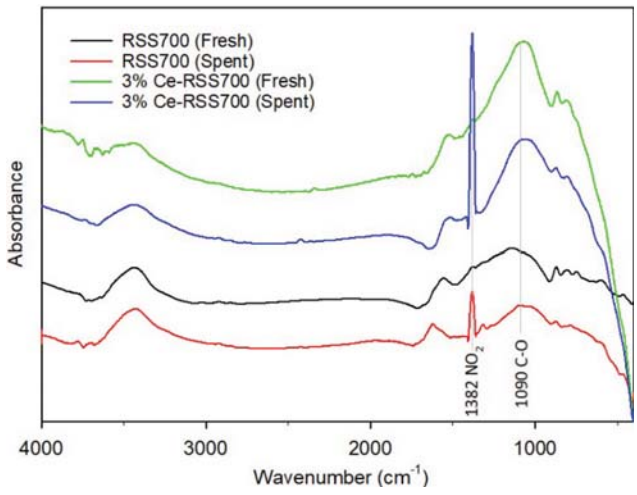

Fig. 5. FTIR spectra of RSS700 and 3% Ce-RSS700 before (fresh) and after (spent) NO adsorption.

biochars indicates that the intensity of the peak existing around 1,090 cm^{-1} increased after loading of Ce on the biochar surface; this indicates the presence of higher amount of oxygen atom on the biochar surface after Ce doping. Also, the comparison of the FTIR spectra between fresh and spent samples, either for pristine or Ce-loaded biochars, reveals the appearance of a very sharp band around 1,382 cm^{-1} in the spectra of spent samples, attributed to the vibration of new species formed by the adsorption of NO on biochar surface. According to the literature [13], this newly appeared peak could be associated with the stretching vibrations of N-O and N=O bands in -O-N=O. This signifies that the species formed by the adsorption of NO on the biochar surface was most probably in the form of C-O-N=O. According to this result, it is possible that NO is adsorbed in the pores as NO_2.

To study the surface composition and to determine the element concentration on biochar surface, XPS analysis was carried out. The high resolution O 1s spectra are shown in Fig. 6. The O 1s spectra can be separated into three peaks: the ones at binding energy of 530.4-531.2 eV which correspond to the C=O groups (peak 1), the peaks at binding energy of 531.6-532.7 eV that are attributed to the C-OH and/or C-O-C groups (peak 2), and the ones at binding energy of 532.4-534.8 eV which are assigned to chemisorbed oxygen [13]. The results of deconvolution of O 1s spectra, as summarized in Table 2, indicate that in pristine biochar (RSS700) most

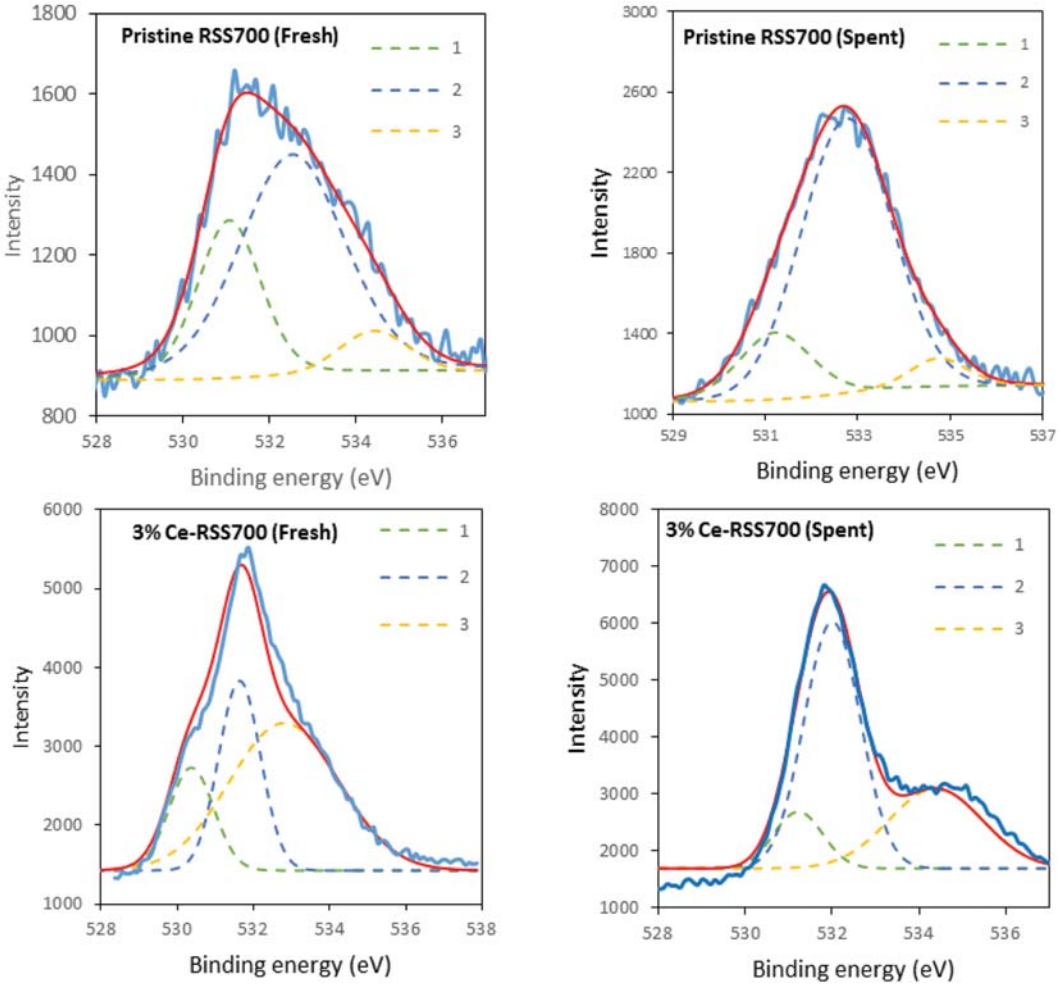

Fig. 6. XPS analysis of O 1s core level for pristine RSS700 and 3% Ce-RSS700 before (fresh) and after (spent) NO adsorption: (1) C=O, (2) C-O and (3) chemisorbed oxygen.

Table 2. Deconvoluted XPS results for O 1s of biochar samples

Samples	Binding energy (relative peak area), eV (%)		
	C=O	C-O	Chemisorbed O
Pristine RSS700 (fresh)	531.1 (27.8)	532.5 (64.8)	534.4 (7.4)
Pristine RSS700 (spent)	531.2 (14.1)	532.8 (81.3)	534.7 (4.6)
3% Ce-RSS700 (fresh)	530.4 (16.0)	531.6 (27.7)	532.8 (56.3)
3% Ce-RSS700 (spent)	531.2 (11.5)	532.0 (57.5)	534.4 (31.0)

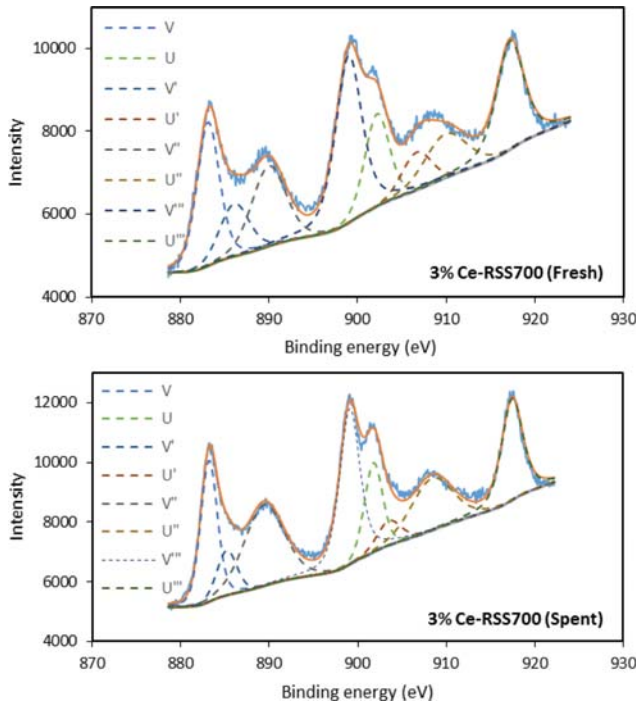

Fig. 7. XPS analysis of Ce 3d core level for pristine RSS700 and 3% Ce-RSS700 before (fresh) and after (spent) NO adsorption.

of oxygen atom (65%) presented in the form of C-O, which agrees with the FTIR result which revealed a strong peak around 1,160 cm^{-1} attributing to the C-O groups. After introduction of cerium into the biochar (3% Ce-RSS700), however, the proportion of chemisorbed oxygen increased considerably. It is well understood that chemisorbed oxygen, which has high mobility, is an active species in catalytic oxidation of NO to NO_2 [23-25]. Hence, the high concentration of chemisorbed oxygen (56%) on CeO_2 loaded biochar could make a great contribution to the adsorption performance. Accordingly, the NO adsorption capacity of 3% Ce-RSS700 was several times higher than that of pristine RSS700.

The Ce 3d core level spectra of 3% Ce-RSS700 before and after NO adsorption are depicted in Fig. 7. The peaks named V, V″, U, U″ and U′″ denote Ce^{4+} and the peaks labeled V′ and U′ represent Ce^{3+} [13,23]. The co-existence of Ce^{3+} and Ce^{4+} is indicative of high redox capability and excellent oxygen storage ability of CeO_2, which is extremely important for catalytic oxidation of NO. The Ce^{3+} species could generate oxygen vacancies, resulting in the formation of chemisorbed oxygen on the biochar surface which could actively contribute to the NO oxidation [23,24]. The deconvolution results presented in Table 2 indicate that for both pristine and CeO_2-loaded biochar, after exposure to NO, the proportion of C=O decreased, while the share of C-O increased significantly. This increase in the proportion of C-O after adsorption could indicate that the adsorbed species on the biochar surface was in the form of C-O-N=O, as proposed based on the FTIR results.

According to the results of experiments and characterizations, a possible mechanism for NO adsorption on Ce-loaded biochar is proposed. Introduction of Ce onto the biochar surface increases the surface adsorbed oxygen [13]:

$$Ce^{4+}-O \rightarrow Ce^{3+}-V_o+O(ad) \quad (1)$$

where the redox cycle between Ce^{4+} and Ce^{3+} releases and stores O atoms through the formation of oxygen vacancy (V_o) defects right next to the Ce^{3+} cation. The adsorbed oxygen atoms may react with vacant active sites of biochar, denoted as C_f, to form C(O) sites:

$$C_f+O(ad) \rightarrow C(O) \quad (2)$$

Then C(O) which is the reactive surface oxygen complex on the surface of biochar can serve as active site to initiate the reaction with gas phase NO:

$$NO(g)+C(O) \rightarrow C-NO_2(ad) \quad (3)$$

Although the extent of physisorption of NO on biochar is generally very low as prior discussed, yet there is a possibility that NO adsorb directly on the vacant active sites of biochar through physical adsorption:

$$NO(g)+C_f \rightarrow C-NO(ad) \quad (4)$$

Then the oxidation of NO to adsorbed NO_2 proceeds through ion pair formation between the adsorbed NO and oxygen species, following a Langmuir-Hinshelwood type reaction, to form physically bound NO_2 and release an active site for the adsorption of subsequent adsorbate molecules [7,11]:

$$C-NO(ad)+C(O) \rightarrow C-NO_2(ad)+C_f \quad (5)$$

The decomposition of surface adsorbed NO_2 occurs at temperatures above 200 °C, where the reduction of C–O–NO releases NO and the concentration of C=O groups may increase [5]:

$$C-NO_2 \xrightarrow{T\uparrow} C(O)+NO \quad (6)$$

The generated C(O) groups are, however, unstable and continue to decompose according to the following reaction [6]:

$$C-C(O) \rightarrow CO+C_f \quad (7)$$

To investigate the regeneration behavior of the sorbent, 3% Ce-RSS700 was subjected to cyclic NO uptake (30 °C) and NO_2 desorption (220 °C) tests. Fig. 8 illustrates the uptake performance of the

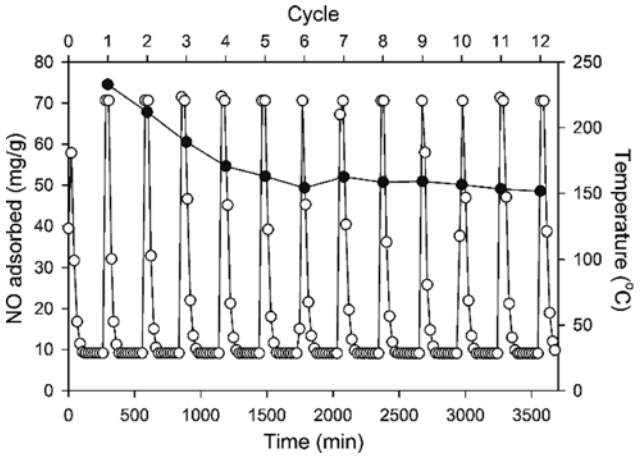

Fig. 8. Cyclic performance of 3% Ce-RSS700 for adsorption of NO; adsorption at 30 °C and desorption at 220 °C.

biochar within twelve temperature swing adsorption-desorption cycles. The temperature-induced desorption could not fully regenerate the biochar to its initial uptake capacity. After 12 cycles, about 68% of the NO_2 in the biochar could be reversibly desorbed, that is, approximately 32% of the initial capacity was lost after 3,550 min of operation. This behavior indicates that different adsorption sites were located on the surface of biochar which could reversibly or irreversibly adsorb the species. It seems the concentration of these irreversible NO_2 adsorption sites did not change considerably after cycle 6 where a relatively stable NO_2 uptake capacity was observed.

3. Kinetic Studies

To describe the kinetics of NO adsorption on biochar and to determine the possible uptake mechanism, three kinetic models, including pseudo-second order, Avrami and Elovich, were used. Pseudo-second order kinetic model, which is more suitable to describe the chemisorption of adsorbate on the adsorbent, presumes that chemical interaction between the gas and solid surface governs the adsorption mechanism [26]:

$$\frac{dq_t}{dt} = k_2(q_e - q_t)^2 \tag{8}$$

where k_2 is the second-order kinetic constant (g/mg·min) and q_e and q_t are the equilibrium and instantaneous adsorption capacity (mg/g), respectively. With the boundary conditions of q_t=0 at t=0 and q_t=q_e at t=t_∞, integrating Eq. (8) gives:

$$q_t = \frac{q_e^2 k_s t}{1 + q_e k_s t} \tag{9}$$

The Avrami kinetic model is usually used to predict the adsorption processes wherein both the physisorption and chemisorption contribute to the overal adsorption process, especially in case of functionalized adsorbents [27]:

$$\frac{dq}{dt} = k_A^{n_A} t^{n_A - 1}(q_e - q_t) \tag{10}$$

where k_A is the Avrami kinetic constant (min^{-1}) and n_A is the Avrami exponent that is often in fractional form. The integrated form of Eq. (10) is:

$$q_t = q_e(1 - e^{-(k_A t)^{n_A}}) \tag{11}$$

The Elovich equation is another useful model to describe the chemisorption of gases on solid adsorbents, without desorption of products. This model assumes that increase in the surface coverage with time can decrease the reaction rate [28]:

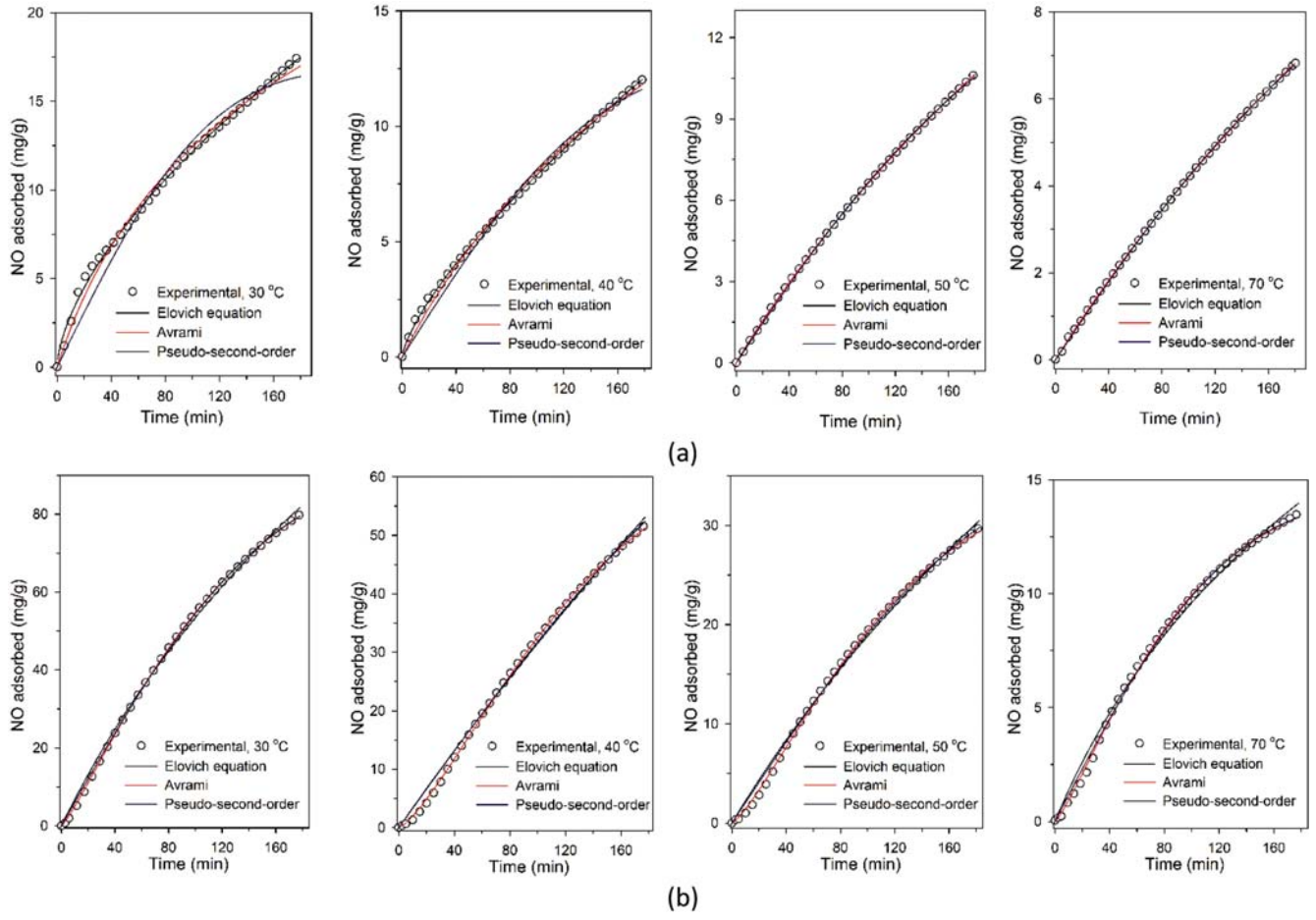

Fig. 9. Plots of pseudo-second order, Avrami and Elovich kinetic models for adsorption of NO on (a) pristine RSS700 and (b) 3% Ce-RSS700 at different adsorption temperatures.

Table 3. Kinetic parameters of Elovich model and regression coefficients for adsorption of NO on pristine and Ce-loaded biochars

Temperature (°C)	Pristine RSS700				3% Ce-RSS700			
	30	40	50	70	30	40	50	70
α (mg/g·min)	0.2428	0.1174	0.0803	0.0487	0.6976	0.3477	0.2260	0.1449
β (g/mg)	0.0976	0.0894	0.0548	0.0718	0.0097	0.0046	0.0190	0.0801
R^2	0.9935	0.9967	0.9999	0.9999	0.9977	0.9955	0.9954	0.9943

$$\frac{dq_t}{dt} = \alpha \exp(-\beta q_t) \quad (12)$$

where α (mg/g.min) and β (g/mg) are model constants. Since dq_t/dt approaches α when $q_t \rightarrow 0$, α can be regarded as the initial reaction rate [28,29]. With the boundary conditions of $q_t=0$ at t=0 and $q_t=q_t$ at t=t and upon integration one obtains [30]:

$$q_t = (1/\beta)\ln(1+\alpha\beta t) \quad (13)$$

In the pseudo-second order and Avrami kinetic models, the driving force is a power of $(q_e - q_t)$ which shows how far the system is from its equilibrium. The Elovich equation, however, includes the driving force in the form of an exponential decay factor where the adsorption rate (dq_t/dt) can only be zero at $q_\infty=\infty$ [31]. By theory this means that there is no limit to the amount of adsorbed gas and hence there is no adsorption plateau.

Fig. 9 shows the use of the three kinetic models to the NO adsorption on pristine and 3% Ce-loaded RSS700 and different temperatures. As observed, all models could well represent the adsorption data; the regression coefficients were quite high (>0.97) for all models. This may signify that chemisorption was the chief controlling mechanism of the adsorption process.

It is most probable that surface oxygen complexes chemically reacted with NO to form C-NO_2; thus chemisorption was the governing mechanism of the adsorption. Among the three kinetic models, the Elovich equation shows a slow chemisorption process that does not have an adsorption plateau, i.e., it does not reach to the saturation point of the adsorbent. Considering that the experimental adsorption data, either for pristine or Ce-loaded biochar, do not approach an asymptotic value within 180 min of adsorption as shown in Figs. 1 and 4, the Elovich equation could be a better model to describe the kinetics of adsorption. The kinetic parameters of this model are presented in Table 3. The values of α, which can be regarded as the reaction rate constant, were lower for pristine biochar compared to those of Ce-doped biochar. With increase of the chemisorption temperature, the value of α decreased. This could be attributed to the exothermic nature of the reaction that resulted in less NO uptake at higher temperatures. This decrease in the value of α with increase of the adsorption temperature yields a negative activation energy, most probably due to the reversible nature of NO adsorption [32]. The reversibility of the NO uptake process was confirmed by cyclic tests as depicted in Fig. 8.

The parameters α and β in the Elovich equation are both dependent on the temperature, particularly, the relation $\ln(\alpha)=C+D/T$ with constants C and D indicates the Arrhenius dependence of α to the reaction temperature [31]. Accordingly, the plot of $\ln\alpha$ vs 1/T was developed to determine the rough activation energy of the NO adsorption on 3% Ce-RSS700 (Fig. S3). From the slope of the plot, the value of apparent activation energy was calculated to be −45 kJ/mol. As a rule of thumb, the activation energies in physisorption and chemisorption processes are typically in the range of 5-40 and 40-800 kJ/mol, respectively [22]. According to this, the adsorption of NO on the Ce-loaded biochar is controlled by chemisorption, confirming the discussion regarding the dominance of chemisorption as inferred from the kinetic models.

CONCLUSION

Oxidative removal of NO over RSS-derived biochar was investigated. The biochar samples prepared at different pyrolysis temperatures showed different NO uptake capacity, attributed to the structural alterations and surface modifications that took place during the carbonization as shown by Raman, SEM and FTIR analyses. Ceria was then introduced into the RSS700 biochar whose NO adsorption capacity was 17.61 mg/g at 30 °C. Doping of the biochar with Ce considerably enhanced the NO uptake capacity of biochar; 3% Ce-RSS700 showed an adsorption capacity of around 75.59 mg/g at 30 °C, which was more than four-times that of pristine biochar. Such significant improvement in the uptake capacity was attributed to the redox cycle ability of Ce, which could shift between Ce^{4+} and Ce^{3+} to provide more adsorbed oxygen on the biochar surface to create surface oxygen complex; these reactive C(O) sites could consequently react with NO to form NO_2 which is more strongly adsorbed on the surface than NO. Kinetic studies using pseudo-second order, Avrami and Elovich models indicated that chemisorption was the governing mechanism for the NO capture with an activation energy of around −45 kJ/mol. The results of this study highlight the high potential of Ce-loaded biochar as a cost-effective and durable sorbent with high capacity for the removal of NO from flue gas.

ACKNOWLEDGEMENT

This research was supported by the Long-Term Research Grant Scheme 203/PJKIMIA/6720009 from Ministry of Education, Malaysia.

SUPPORTING INFORMATION

Additional information as noted in the text. This information is available via the Internet at http://www.springer.com/chemistry/journal/11814.

REFERENCES

1. M. T. Izquierdo and B. Rubio, *Environ. Sci. Technol.*, **32**, 4017 (1998).

2. X. Tang, F. Gao, Y. Xiang, H. Yi and S. Zhao, *Catal. Commun.*, **64**, 12 (2015).
3. X. Zhang and R. Lin, *Energy Procedia*, **158**, 4805 (2019).
4. F. Gao, C. Chu, W. Zhu, X. Tang, H. Yi and R. Zhang, *Appl. Surf. Sci.*, **479**, 548 (2019).
5. Y. Guo, Y. Li, T. Zhu and M. Ye, *Fuel*, **143**, 536 (2015).
6. J. Chen, F. Cao, S. Chen, M. Ni, X. Gao and K. Cen, *Appl. Surf. Sci.*, **317**, 26 (2014).
7. A. Rubel, M. Stewart and J. Stencel, *J. Mater. Res.*, **10**, 562 (1995).
8. X. Wang, X. Xu, S. Liu, Y. Zhang, C. Zhao and F. Yang, *J. Hazard. Mater.*, **312**, 175 (2016).
9. A. M. Rubel and J. M. Stencel, *Energy Fuels*, **10**, 704 (1996).
10. H. Chen, Y. Wang and Y.-K. Lyu, *Mol. Catal.*, **454**, 21 (2018).
11. S. Adapa, V. Gaur and N. Verma, *Chem. Eng. J.*, **116**, 25 (2006).
12. B. C. Enger, X. Auvray, R. Lodeng, M. Menon, D. Waller and M. Ronning, *Appl. Catal., A*, **564**, 142 (2018).
13. F. Cao, J. Chen, M. Ni, H. Song, G. Xiao, W. Wu, X. Gao and K. Cen, *Appl. Surf. Sci.*, **4**, 16281 (2014).
14. D. Stoyanova, P. Georgieva, I. Avramova, K. Aleksieva, D. Marinova and D. Mehandjiev, *J. Rare Earths*, **37**, 151 (2019).
15. M. Y. Mihaylov, E. Z. Ivanova, H. A. Aleksandrov, P. S. Petkov, G. N. Vayssilov and K. I. Hadjiivanov, *Mol. Catal.*, **451**, 114 (2018).
16. C. Fang, D. Zhang, L. Shi, R. Gao, H. Li, L. Ye and J. Zhang, *Catal. Sci. Technol.*, **3**, 803 (2013).
17. A. S. Al-Rahbi and P. T. Williams, *Waste Manag.*, **49**, 188 (2016).
18. F.-T. You, G.-W. Yu, Y. Wang, Z.-J. Xing, X.-J. Liu and J. Li, *Appl. Surf. Sci.*, **413**, 387 (2017).
19. F.-T. You, G.-W. Yu, Z.-J. Xing, J. Li, S.-Y. Xie, C.-X. Li, G. Wang, H.-Y. Ren and Y. Wang, *Appl. Surf. Sci.*, **471**, 633 (2019).
20. Y.-W. Lee, D.-K. Choi and J.-W. Park, *Carbon*, **40**, 1409 (2002).
21. X. Li, Z. Dong, J. Dou, J. Yu and A. Tahmasebi, *Fuel Process. Technol.*, **148**, 91 (2016).
22. S. Sumathi, S. Bhatia, K. Lee and A. Mohamed, *Chem. Eng. J.*, **162**, 51 (2010).
23. W. Wang, R. Guo, W. Pan and G. Hu, *J. Rare Earths*, **36**, 588 (2018).
24. W. Wang, W. Li, R. Guo, Q. Chen, Q. Wang, W. Pan and G. Hu, *J. Rare Earths*, **34**, 876 (2016).
25. X. Yu, X. Wu, Z. Chen, Z. Huang and G. Jing, *Mol. Catal.*, **476**, 110512 (2019).
26. S. N. Kudahi, A. R. Noorpoor and N. M. Mahmoodi, *J. CO_2 Util.*, **21**, 17 (2017).
27. P. Lahijani, M. Mohammadi and A. R. Mohamed, *J. CO_2 Util.*, **26**, 281 (2018).
28. R.-S. Juang and M.-L. Chen, *Ind. Eng. Chem. Res.*, **36**, 813 (1997).
29. F.-C. Wu, R.-L. Tseng and R.-S. Juang, *Chem. Eng. J.*, **150**, 366 (2009).
30. L. Largitte and R. Pasquier, *Chem. Eng. Res.*, **109**, 495 (2016).
31. E. Andreoli, L. Cullum and A. Barron, *Ind. Eng. Chem. Res.*, **54**, 878 (2015).
32. H. Teng and E. M. Suuberg, *J. Phy. Chem.*, **97**, 478 (1993).

Supporting Information

Low temperature adsorption of nitric oxide on cerium impregnated biomass-derived biochar

Shahreen Izwan Anthonysamy*, Pooya Lahijani*, Maedeh Mohammadi, and Abdul Rahman Mohamed*,†**

*Low Carbon Economy (LCE) Research Group, School of Chemical Engineering, Universiti Sains Malaysia, 14300, Nibong Tebal, Pulau Pinang, Malaysia
**Faculty of Chemical Engineering, Babol Noshirvani University of Technology, Babol 47148, Iran
(*Received 17 June 2019 • accepted 12 October 2019*)

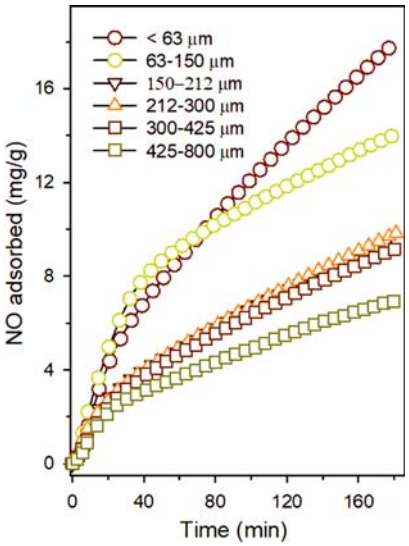

Fig. S1. Effect of particle size of RSS700 biochar on NO adsorption capacity.

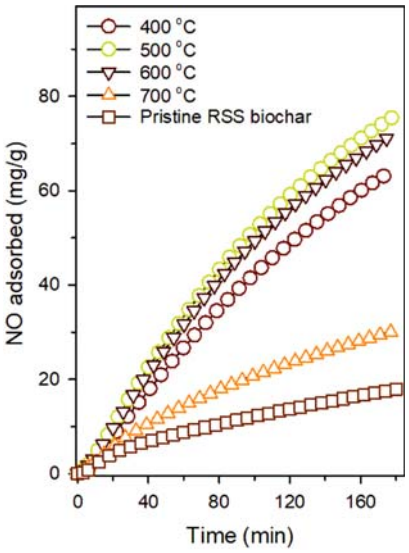

Fig. S2. Effect of calcination temperature on NO adsorption capacity of 3% Ce-RSS700 biochar.

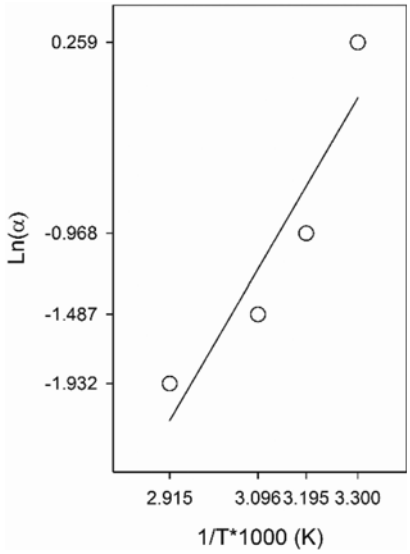

Fig. S3. Arrhenius plot for adsorption of NO on the 3% Ce-RSS700 biochar.